Geometric Multigrid Method for Electro- and Magnetostatic Field Simulations Using the Conformal Finite Integration Technique

Stefan Feigh, Markus Clemens and Thomas Weiland
Technische Universität Darmstadt, FB 18 Elektrotechnik und Informationstechnik,
Computational Electromagnetics Laboratory (TEMF), Schloßgartenstr. 8, D-64289 Darmstadt, Germany
email: feigh/clemens/weiland@temf.tu-darmstadt.de.

Abstract

A geometrical multigrid algorithm for vector based formulations for electromagnetic field problems discretized by the Conformal Finite Integration Technique is proposed. The transfer operators and the coarse grid operators are constructed for a hierarchy of non-nested grids. A validation of the presented approach is achieved for electro-static and magneto-static test problems for which a discrete Poisson and a discrete Curl-Curl equation have to be solved respectively. Experimental results for the asymptotic complexity and for the convergence characteristics in case of discontinuous material coefficients are presented.

I. Introduction

In the field of computational electrodynamics the Finite Integration Technique (FIT) proposed by Weiland [1] is a well established method, which is used in several commercial software packages. The FIT formulation provides a general spatial discretization scheme for the discretization of electromagnetic problems with arbitrary geometries, e.g. static problems or calculations in frequency or time domain and is similar to Finite Difference Methods with vector quantities. The Conformal Finite Integration Technique (C-FIT), first introduced in [2], alleviates the problem of staircasing when material interfaces are not aligned with the grid, by introducing a mesh independent boundary resolution technique. A geometrical multigrid solver for scalar and vector based formulations of this C-FIT method is presented for non-nested Cartesian tensor-product grids and tested for Poisson and Curl-Curl equations related to electro-static and magneto-static problems, respectively. The Cartesian tensor-product grid structure leads to simple structured matrices and fast matrix-vector multiplications compared to those related to unstructured grids which are commonly used in Finite Element Methods, while still featuring good discretization qualities due to the C-FIT approach. Numerical investigations are performed to analyze the convergence properties of the developed multigrid solver for both Poisson and Curl-Curl equations.

II. The Finite Integration Technique (FIT)

In the FIT, Maxwell's equations in their integral form and the constitutive material relations are mapped onto a dual-orthogonal, staggered grid system $\{\mathbf{G}, \widetilde{\mathbf{G}}\}$. The grid $\mathbf{G}$ is referred to as the primary grid containing vertices N_i, edges L_i, facets A_i and volumes V_i, whereas $\widetilde{\mathbf{G}}$ is referred to as the dual grid consisting of vertices $\widetilde{N}_i$, edges $\widetilde{L}_i$, facets $\widetilde{A}_i$ and volumes $\widetilde{V}_i$. Here, only Cartesian tensor-product grids are considered. The so-called metric matrices contain the information of this grid system and are defined by

$$\mathbf{D}_L = \mathrm{diag}\{|L_i|\}_{i\,:\,L_i\in\mathbf{G}} \;;\; \mathbf{D}_A = \mathrm{diag}\{|A_i|\}_{i\,:\,A_i\in\mathbf{G}} \;,\; \widetilde{\mathbf{D}}_L = \mathrm{diag}\{|\widetilde{L}_i|\}_{i\,:\,\widetilde{L}_i\in\widetilde{\mathbf{G}}} \;;\; \widetilde{\mathbf{D}}_A = \mathrm{diag}\{|\widetilde{A}_i|\}_{i\,:\,\widetilde{A}_i\in\widetilde{\mathbf{G}}}.$$

Instead of field quantities, integral state variables are used to formulate the problem. The *electric voltage* $\widehat{e}$, *magnetic voltage* $\widehat{h}$, *electric flux* $\widehat{\widehat{d}}$ and *magnetic flux* $\widehat{\widehat{b}}$ are defined by line integrals of the elementary field values $\vec{E}$ (electric field), $\vec{H}$ (magnetic field), and integrals over cell facets of $\vec{D}$ (electric flux density) and $\vec{B}$ (magnetic flux density),

$$\widehat{e}_i = \int_{L_i} \vec{E}\cdot d\vec{s}, \qquad \widehat{h}_i = \int_{\widetilde{L}_i} \vec{H}\cdot d\vec{s}, \qquad \widehat{\widehat{d}}_i = \int_{\widetilde{A}_i} \vec{D}\cdot d\vec{A}, \qquad \widehat{\widehat{b}}_i = \int_{A_i} \vec{B}\cdot d\vec{A}.$$

S. Feigh is supported by the graduate student programme 'Physik und Technik von Teilchenbeschleunigern of the Deutsche Forschungsgemeinschaft (DFG) under grant GK-GRK 410/1.

The components are gathered into the vectors $\widehat{\mathbf{e}} = \{\widehat{e}_i\}$, $\widehat{\mathbf{h}} = \{\widehat{h}_i\}$, $\widehat{\widetilde{\mathbf{d}}} = \{\widehat{\widetilde{d}}_i\}$ and $\widehat{\widetilde{\mathbf{b}}} = \{\widehat{\widetilde{b}}_i\}$. Furthermore, the current density $\vec{J}$, the charge density Q, the electric potential Φ and the magnetic vector potential $\vec{A}$ are mapped onto the dual grid, i.e.,

$$\widehat{\widetilde{j}}_i = \int_{\widetilde{A}_i} \vec{J} \cdot d\vec{A} \quad , \quad q_i = \int_{\widetilde{V}_i} Q dV \quad , \quad \phi_i = \Phi|_{N_i} \quad \text{and} \quad \widehat{a}_i = \int_{L_i} \vec{A} \cdot d\vec{s},$$

and are collected in the vectors $\widehat{\widetilde{\mathbf{j}}} = \{\widehat{\widetilde{j}}_i\}$, $\mathbf{q} = \{\mathbf{q_i}\}$, $\phi = \{\phi_i\}$ and $\widehat{\mathbf{a}} = \{\widehat{a}_i\}$.

A. Maxwell Grid Equations (MGE)

The integral state variables are allocated at the simplicial elements of the primary or dual grid: $\widehat{e}$ at edges, $\widehat{\widetilde{b}}$ at facets of the primary grid $\mathbf{G}$, and $\widehat{h}$ at edges, $\widehat{\widetilde{d}}$ at facets of the dual grid $\widetilde{\mathbf{G}}$, respectively. This procedure enables the discretization of Maxwell's equations in a straightforward way. Using the integral formulation of Maxwell's equations on the introduced dual orthogonal grid system $\{\mathbf{G}, \widetilde{\mathbf{G}}\}$ a set of matrix equations, the so-called Maxwell Grid Equations (MGE), can be derived:

$$\int_A (\nabla \times \vec{E}) \cdot d\vec{A} = \int_{\partial A} \vec{E} \cdot d\vec{s} = -\int_A \frac{\partial}{\partial t} \vec{B} \cdot d\vec{A} \quad \Longrightarrow \quad \mathbf{C}\widehat{\mathbf{e}} = -\frac{d}{dt}\widehat{\widetilde{\mathbf{b}}} \tag{1}$$

$$\int_{\widetilde{A}} (\nabla \times \vec{H}) \cdot d\vec{A} = \int_{\partial \widetilde{A}} \vec{H} \cdot d\vec{s} = \int_{\widetilde{A}} \left(\frac{\partial}{\partial t}\vec{D} + \vec{J}\right) \cdot d\vec{A} \quad \Longrightarrow \quad \widetilde{\mathbf{C}}\widehat{\mathbf{h}} = \frac{d}{dt}\widehat{\widetilde{\mathbf{d}}} + \widehat{\widetilde{\mathbf{j}}} \tag{2}$$

$$\int_V (\nabla \cdot \vec{B}) \ dV = \int_{\partial V} \vec{B} \cdot d\vec{A} = 0 \quad \Longrightarrow \quad \mathbf{S}\widehat{\widetilde{\mathbf{b}}} = \mathbf{0} \tag{3}$$

$$\int_{\widetilde{V}} (\nabla \cdot \vec{D}) \ dV = \int_{\partial \widetilde{V}} \vec{D} \cdot d\vec{A} = \int_{\widetilde{V}} Q \ dV \quad \Longrightarrow \quad \widetilde{\mathbf{S}}\widehat{\widetilde{\mathbf{d}}} = \mathbf{q} \tag{4}$$

The operators $\mathbf{C}, \widetilde{\mathbf{C}}$ and $\mathbf{S}, \widetilde{\mathbf{S}}$ are the discrete analogues to the *curl* and *divergence* operators of the continuous formulation for the primary and dual grid, respectively. They correspond to the exact summation for closed line integrals $\mathbf{C}$, $\widetilde{\mathbf{C}}$ or closed surface integrals $\mathbf{S}$, $\widetilde{\mathbf{S}}$ on $\{\mathbf{G}, \widetilde{\mathbf{G}}\}$ and thus provide the topological relations inducted by Maxwell's integral equations applied to the grid set. The discrete operators $\mathbf{C}, \widetilde{\mathbf{C}}, \mathbf{S}, \widetilde{\mathbf{S}}$, also denoted as topological operators, are incidence matrices and depend only on the grid structure. Their algebraic properties

$$\mathbf{SC} = 0 \quad , \quad \widetilde{\mathbf{S}}\widetilde{\mathbf{C}} = 0 \quad , \quad \mathbf{C}\widetilde{\mathbf{S}}^T = 0 \quad \text{and} \quad \widetilde{\mathbf{C}}\mathbf{S}^T = 0,$$

mimic their analytical counterparts div curl $\equiv 0$ and curl grad $\equiv 0$ and are necessary conditions for the consistency of the FIT formulation. Based on the concept of grid voltages and grid fluxes, the MGE represent an exact transformation of the continuous Maxwell equations onto $\{\mathbf{G}, \widetilde{\mathbf{G}}\}$.

B. Discrete Constitutive Relations

In the next step the continuous constitutive relations are discretized yielding the relations

$$\vec{D} = \varepsilon \vec{E} \implies \widehat{\widetilde{\mathbf{d}}} = \mathbf{M}_\varepsilon \widehat{\mathbf{e}} \quad , \quad \vec{H} = \nu \vec{B} \implies \widehat{\mathbf{h}} = \mathbf{M}_\nu \widehat{\widetilde{\mathbf{b}}} \quad \text{and} \quad \vec{J} = \kappa \vec{E} \implies \widehat{\widetilde{\mathbf{j}}} = \mathbf{M}_\kappa \widehat{\mathbf{e}}. \tag{5}$$

Here, permanent electric and magnetic polarizations are neglected. The material matrices $\mathbf{M}_\nu$, $\mathbf{M}_\varepsilon$ and $\mathbf{M}_\kappa$ represent the discrete reluctivity, permittivity and conductivity matrices, respectively. Before applying the continuous material relation, the integral state variables have to be transformed into their corresponding average fi eld quantities. Then the averaged fi eld components are transformed, using an averaged material coeffi cient, into their corresponding integral state variables according to

$$\widehat{e}_i \xrightarrow{\frac{1}{|L_i|}} \overline{\vec{E}}_i \xrightarrow{\overline{\varepsilon}_i} \overline{\vec{D}}_i \xrightarrow{|\widetilde{A}_i|} \widehat{\widetilde{d}}_i \quad , \quad \widehat{e}_i \xrightarrow{\frac{1}{|L_i|}} \overline{\vec{E}}_i \xrightarrow{\overline{\kappa}_i} \overline{\vec{J}}_i \xrightarrow{|\widetilde{A}_i|} \widehat{\widetilde{j}}_i \quad , \quad \widehat{\widetilde{b}}_i \xrightarrow{\frac{1}{|A_i|}} \overline{\vec{B}}_i \xrightarrow{\overline{\nu}_i} \overline{\vec{H}}_i \xrightarrow{|\widetilde{L}_i|} \widehat{h}_i \ . \tag{6}$$

The material coeffi cients used in (6) are averaged over the simplices at which the corresponding fi eld quantities are defi ned:

$$\overline{\varepsilon}_i = \frac{\int_{\widetilde{A}_i} \varepsilon \ \vec{n}_i \cdot d\vec{A}}{|\widetilde{A}_i|} \quad , \quad \overline{\kappa}_i = \frac{\int_{\widetilde{A}_i} \kappa \ \vec{n}_i \cdot d\vec{A}}{|\widetilde{A}_i|} \quad , \quad \overline{\nu}_i = \frac{\int_{A_i} \nu \ \vec{m}_i \cdot d\vec{A}}{|A_i|}, \tag{7}$$

where $\vec{n}_i$ is a unit normal vector at $\widetilde{A}_i$ and $\vec{m}_i$ is a unit normal vector at A_i, respectively. The complete transformation procedure for all components of the integral state variables can now be written in matrix notation

$$\widehat{\widetilde{\mathbf{d}}} = \underbrace{\widetilde{\mathbf{D}}_A \mathbf{D}_\varepsilon \mathbf{D}_L^{-1}}_{\mathbf{M}_\varepsilon :=} \widehat{\mathbf{e}} \quad , \quad \widehat{\widetilde{\mathbf{j}}} = \underbrace{\widetilde{\mathbf{D}}_A \mathbf{D}_\kappa \mathbf{D}_L^{-1}}_{\mathbf{M}_\kappa :=} \widehat{\mathbf{e}} \quad , \quad \widehat{\mathbf{h}} = \underbrace{\widetilde{\mathbf{D}}_L \mathbf{D}_\nu \mathbf{D}_A^{-1}}_{\mathbf{M}_\nu :=} \widehat{\mathbf{b}},$$

where

$$\mathbf{D}_\varepsilon = \mathrm{diag}\{\overline{\varepsilon}_i\}_{i\,:\,\widetilde{A}_i \in \widetilde{\mathbf{G}}} \quad , \quad \mathbf{D}_\kappa = \mathrm{diag}\{\overline{\kappa}_i\}_{i\,:\,\widetilde{A}_i \in \widetilde{\mathbf{G}}} \quad \text{and} \quad \mathbf{D}_\nu = \mathrm{diag}\{\overline{\nu}_i\}_{i\,:\,A_i \in \mathbf{G}}.$$

The material matrices are diagonal and thus represent a one to one relation between the integral state quantities which is a consequence of the fact that the primary and dual grid intersect each other orthogonally. The introduction of the Conformal Finite Integration Technique was first proposed in [2] and [3] independently. In extension of the classical FIT [1] it is using an exact numerical evaluation of the integrals in (7) instead of a trivial approximation. It appropriately considers curved material interfaces inside the cells of $\mathbf{G}$ (see Fig. 1 for $\overline{\varepsilon}$). With this method an easy to generate Cartesian grid structure, which leads to simple and numerically efficient structured matrix equations, can be used, even for problems with curved material boundary interfaces and complicated shape boundaries.

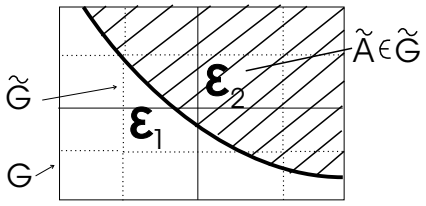

Fig. 1. Discretization of material distribution in the C-FIT.

The discrete constitutive relations complete the Maxwell Grid Equations to handle electromagnetic problems in the discrete grid space. The accuracy of the algorithm is discussed in [8]. Recent publications on geometric discretization methods for Maxwell's equations show that lowest order Whitney-Finite Element formulations can be denoted in the form of (1) - (4) as well, where the main difference between these methods lies in the construction principle of the material matrices $\mathbf{M}_\varepsilon$, $\mathbf{M}_\kappa$ and $\mathbf{M}_\nu$ [4].

III. MULTIGRID

Multigrid (MG) solvers contain two basic components, i.e., error smoothing operations and a coarse grid correction procedure. A two grid cycle [5] for the solution of the linear system $\mathbf{A}_h u_h = f_h$ is depicted in Fig. 2. The lower index refers to the grid level and the upper index to the iteration number. In the first step the high frequency components of the error of a solution vector u_h^m are eliminated by a (pre-)smoothing method such as damped Jacobi or Gauss-Seidel relaxation. The index β indicates the number of relaxation steps. The defect $\overline{d}_h^m = f_h - \mathbf{A}_h \overline{u}_h^m$ of the smoothed solution $\overline{u}_h^m$ is projected onto a coarser grid by a restriction operator $\mathbf{R}_h$. Using the projected problem matrix $\mathbf{A}_{h+1}$ the correction on the coarse grid is obtained by a direct solution method, or by the same two-grid cycle mechanism, applied to solve the correction equation recursively if the coarse grid system is still too large to be solved directly. The obtained correction vector v_{h+1}^m is interpolated back onto the fine grid by a prolongation operator $\mathbf{P}_h$. The fine grid correction

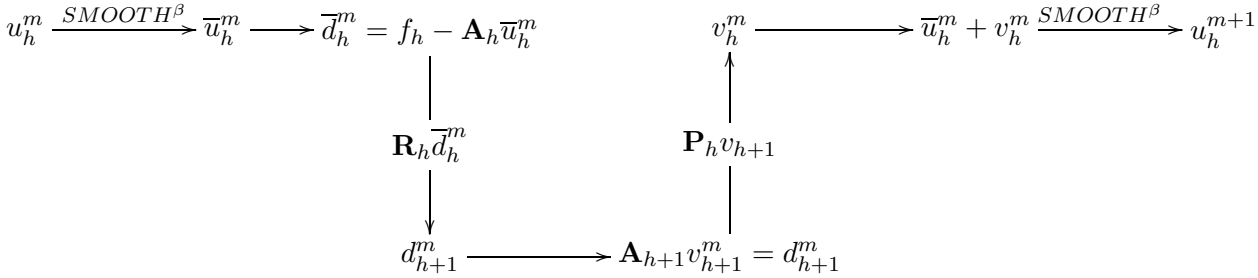

Fig. 2. Two-grid cycle.

v_h^m is added to the old solution and finally a (post-) smoothing method is applied to get rid of the high frequency errors introduced by the prolongation. This coarse grid correction reduces the low frequency error components.

The ingredients for this MG solver are the grid transfer operators ($\mathbf{R}_h$ and $\mathbf{P}_h$) and the operators of the projected problem $\mathbf{A}_h$ for all grid levels. These grid transfer operators will be constructed based on geometrical considerations and thus they are different for voltage, flux or volume quantities. Furthermore, a relation $\mathbf{R} = \mathbf{P}^T$ will not result in a consistent geometrical projection method and therefore was not used for the construction of the transfer operators. The construction of the transfer operators is substantially easier to define for tensor-product grids which are considered with the C-FIT than for general unstructured grids. Furthermore, the grid $\{\mathbf{G}_{h+1}, \widetilde{\mathbf{G}}_{h+1}\}$ is constructed such that the edges $L_{h+1,i} \in \mathbf{G}_{h+1}$ are either parallel or perpendicular to the edges $L_{h,i} \in \mathbf{G}_h$, which simplifies the construction of the transfer operators as well. The generation of the meshes $\{\mathbf{G}_h, \widetilde{\mathbf{G}}_h\}$ on the different grid levels, however, is non-trivial in the case when problems with large jumps in the material coefficients have to be solved. Here, the material interface surfaces have to be taken into account in a special way, which means that at each grid level the grid points should preferably lie on those boundary surfaces [5].

In the next two subsections no distinction between primary and dual variables is made, since there is no essential difference in the construction principle of the transfer operators. Furthermore, the values of integral state variables allocated at edges L, facets A and volumes V are denoted by $\widehat{L}$, $\widehat{\widehat{A}}$ and $\widehat{\widehat{\widehat{V}}}$ respectively. The length of an edge L will be referred to as $|L|$, the area of an facet A will be denoted as $|A|$ and the volume of a cell V will be written as $|V|$. N_h denotes the number of grid vertices N.

A. Construction of Restriction Operators

Since the grids are non-nested, the grid points of the coarse mesh do not have to match grid points of the fine mesh. The geometry for the construction of the restriction operators $\mathbf{R}_L$ for edges quantities is sketched in Fig. 3. The edges L_{h+1} do not necessarily lie on old edges L_h. Hence an average over the four nearest edges is computed. In this approach

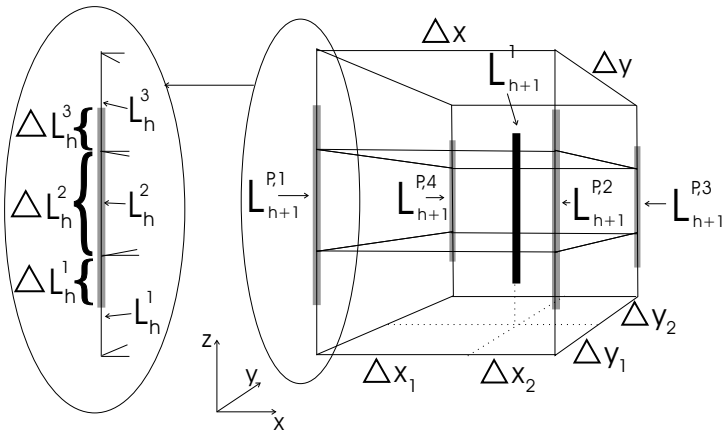

Fig. 3. Restriction of integral state variables allocated on edges

the average value is derived with respect to the distance to the new edge using a linear interpolation algorithm

$$\widehat{L}^1_{h+1} = w^x_1 w^y_1 \widehat{L}^{P,1}_{h+1} + w^x_2 w^y_1 \widehat{L}^{P,2}_{h+1} + w^x_2 w^y_2 \widehat{L}^{P,3}_{h+1} + w^x_1 w^y_2 \widehat{L}^{P,4}_{h+1}, \tag{8}$$

with the factors

$$w^x_i = \frac{\Delta x - \Delta x_i}{\Delta x} \quad \text{and} \quad w^y_i = \frac{\Delta y - \Delta y_i}{\Delta y}.$$

The projected edges $L^{P,i}_{h+1}$ are constructed from edges or fractions of edges L^j_h of the fine grid L_h. A linear weighting with respect to the overlap was chosen to determine $\widehat{L}^{P,i}_{h+1}$, e.g. $\widehat{L}^{P,1}_{h+1}$ in Fig. 3 is derived by $\widehat{L}^{P,1}_{h+1} = w^z_1 \widehat{L}^1_h + w^z_2 \widehat{L}^2_h + w^z_3 \widehat{L}^3_h$ and in general

$$\widehat{L}^{P,1}_{h+1} = \sum_{L^j_h \text{ overlapping } L^{P,i}_{h+1}} w^z_j \widehat{L}^j_h,$$

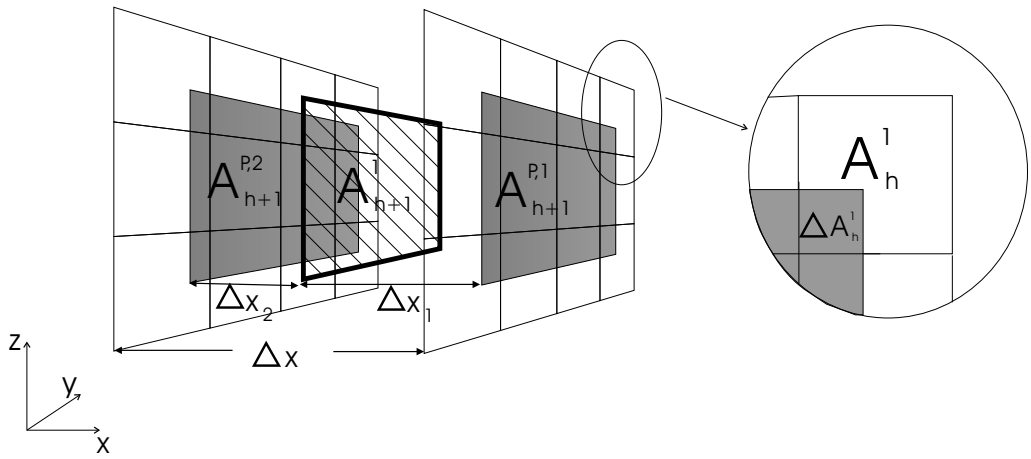

Fig. 4. Restriction of integral state variables allocated on facets

where $w_j^z = \frac{\Delta L_h^j}{|L_h^j|}$. A similar projection method is developed for the construction of the restriction operators $\mathbf{R}_A$ of facet quantities (Fig. 4). In this case the new facet lies between old facets. Therefore, the new facet has to be interpolated using the old facets. Similar to the construction of the projection of edges a linear interpolation procedure is applied with

$$\widehat{\widehat{A}}_{h+1}^1 = w_1^x \widehat{\widehat{A}}_{h+1}^{P,1} + w_2^x \widehat{\widehat{A}}_{h+1}^{P,2}, \tag{9}$$

where $w_i^x = \frac{\Delta x - \Delta x_i}{\Delta x}$. The projected facets $A_{h+1}^{P,i}$ are composed of facets and fractions of facets A_h^j respectively, of the fine grid A_h. Again a linear weighting with respect to the overlapping area is applied to determine $\widehat{\widehat{A}}_{h+1}^{P,i}$

$$\widehat{\widehat{A}}_{h+1}^{P,i} = \sum_{A_h^j \text{ overlapping } A_{h+1}^{P,i}} w_j^A \widehat{\widehat{A}}_h^j,$$

where $w_j^A = \frac{\Delta A_h^j}{|A_h^j|}$. According to this projection properties the restriction operators $\mathbf{R}_L$, $\widetilde{\mathbf{R}}_L$, $\mathbf{R}_A$, $\widetilde{\mathbf{R}}_A : \mathbb{R}^{3N_h \times 3N_h} \rightarrow \mathbb{R}^{3N_{h+1} \times 3N_{h+1}}$ can be constructed. The construction of the restriction operators $\mathbf{R}_V$, $\widetilde{\mathbf{R}}_V$ for volume quantities does not involve an geometrical projection as in (8) and (9). All new cells V_{h+1} are composed of fractions of old cells with the volume ΔV_h^j. The restriction operator is constructed, such that

$$\widehat{\widehat{V}}_{h+1} = \sum_{V_h^j \text{ overlapping } V_{h+1}} w_j^V \widehat{\widehat{V}}_h^j,$$

where $w_j^V = \frac{\Delta V_h^j}{|V_h^j|}$. For the restriction operator $\mathbf{R}_N$ of the variables allocated on nodes, e.g. ϕ, a linear interpolation scheme was used to obtain the values on the coarse grid. In this way the restriction operators $\mathbf{R}_V$, $\widetilde{\mathbf{R}}_V$, $\mathbf{R}_N$, $\widetilde{\mathbf{R}}_N$: $\mathbb{R}^{N_h \times N_h} \rightarrow \mathbb{R}^{N_{h+1} \times N_{h+1}}$ can be constructed.

B. Construction of Prolongation Operators

The construction of the prolongation operators is similar to that of the restriction operators. The unknown fine grid quantities have to be interpolated from the coarse grid quantities. The geometry for the construction of the prolongation operators $\mathbf{P}_L$ for edge quantities, is sketched in Fig. 5. The four closest edge quantities of the coarse grid are projected on the edges of the fine grid by the linear interpolated scheme

$$\widehat{L}_{h+1}^P = w_1^y w_1^x \widehat{L}_{h+1}^1 + w_1^y w_2^x \widehat{L}_{h+1}^2 + w_2^y w_1^x \widehat{L}_{h+1}^3 + w_2^y w_2^x \widehat{L}_{h+1}^4,$$

with the factors

$$w_i^x = \frac{\Delta x - \Delta x_i}{\Delta x} \quad \text{and} \quad w_i^y = \frac{\Delta y - \Delta y_i}{\Delta y}.$$

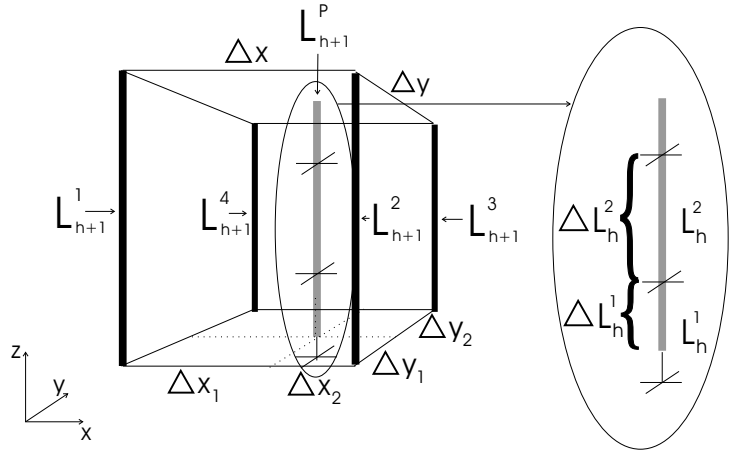

Fig. 5. Prolongation of integral state quantities allocated on edges.

In the next step the projected quantity $\widehat{L}^P_{h+1}$ is divided according to the lengths of the edges of the fine grid L^j_h overlapping with L^P_{h+1}

$$\widehat{L}^j_h = \sum_{L^P_{h+1} \text{ overlapping } L^j_h} w^z_j \widehat{L}^P_{h+1},$$

where $w^z_j = \frac{\Delta L^j_h}{|L^P_{h+1}|}$. The prolongation of the facet based quantities is depicted in Fig. 6. The facets of the coarse grid are projected on the fine grid and interpolated according to

$$\widehat{\widehat{A}}^P_{h+1} = w^x_1 \widehat{\widehat{A}}^1_{h,1} + w^x_2 \widehat{\widehat{A}}^2_{h+1},$$

where $w^x_i = \frac{\Delta x - \Delta x_i}{\Delta x}$. The projected facets are composed of facets of the fine grid. Each facet of the fine grid is composed of one, two or four projected facets A^P_{h+1}. The facet quantities of the fine grid are therefore derived by

$$\widehat{\widehat{A}}^j_h = \sum_{A^P_{h+1} \text{ overlapping } A^j_h} w^A_j \widehat{\widehat{A}}^P_{h+1}$$

where $w^A_j = \frac{\Delta A^j_h}{|A^P_{h+1}|}$. In this way the prolongation operators $\mathbf{P}_L$, $\widetilde{\mathbf{P}}_L$, $\mathbf{P}_A$, $\widetilde{\mathbf{P}}_A : \mathbb{R}^{3N_{h+1} \times 3N_{h+1}} \rightarrow \mathbb{R}^{3N_h \times 3N_h}$ can

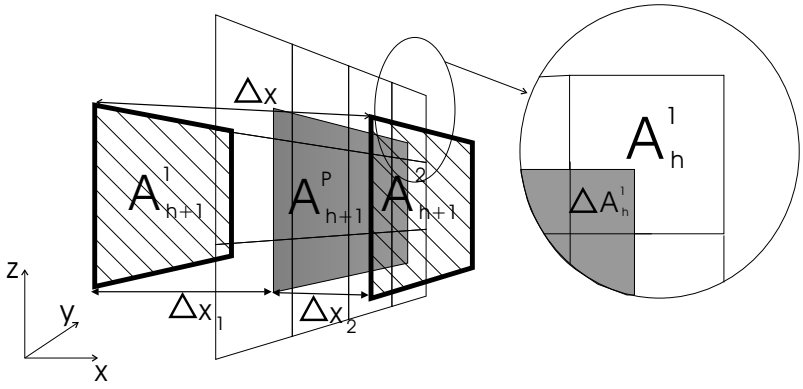

Fig. 6. Prolongation of integral state quantities allocated on facets.

be constructed. Similar to the restriction process the prolongation for the volume quantities does not involve any geometrical projections. The volumes V_h of the fine grid are composed by fractions of volumes ΔV^j_h of the coarse grid. Therefore the prolongation reads

$$\widehat{\widehat{V}}_h = \sum_{V^j_{h+1} \text{ overlapping } V_h} w^V_j \widehat{\widehat{V}}^j_{h+1},$$

where $w_j^V = \frac{\Delta V_h^j}{|V_{h+1}|}$. Again the prolongation operator $\mathbf{P}_N$ for values allocated on nodes is built using a linear interpolation scheme to obtain the fine grid values from the coarse grid values. Accordingly, the prolongation operators $\mathbf{P}_V$, $\widetilde{\mathbf{P}}_V$, $\mathbf{P}_N$, $\widetilde{\mathbf{P}}_N : \mathbb{R}^{N_{h+1} \times N_{h+1}} \rightarrow \mathbb{R}^{N_h \times N_h}$ are constructed.

C. Projection of Problem

The transfer operators developed above can be used to transfer all integral state variables between the different grid levels. An overview is given in the table below. Furthermore the transfer operators can be used to create the geometry

	Vertices N	Edges L	Facets A	Edges $\widetilde{L}$	Facets $\widetilde{A}$	Volumes $\widetilde{V}$
State variables	ϕ	$\widehat{\mathbf{e}}$, $\widehat{\mathbf{a}}$	$\widehat{\widehat{\mathbf{b}}}$	$\widehat{\mathbf{h}}$	$\widehat{\widehat{\mathbf{d}}}$, $\widehat{\widehat{\mathbf{j}}}$	$\mathbf{q}$
Transfer operators	$\mathbf{R}_N$, $\mathbf{P}_N$	$\mathbf{R}_L$, $\mathbf{P}_L$	$\mathbf{R}_A$, $\mathbf{P}_A$	$\widetilde{\mathbf{R}}_L$, $\widetilde{\mathbf{P}}_L$	$\widetilde{\mathbf{R}}_A$, $\widetilde{\mathbf{P}}_A$	$\widetilde{\mathbf{R}}_V$, $\widetilde{\mathbf{P}}_V$

and material matrices of the coarse grids from those of the finest grid. The problem matrix $\mathbf{A}$ is an expression of the material matrices and the incidence matrices

$$\mathbf{A} = f(\mathbf{M}_\varepsilon, \mathbf{M}_\nu, \mathbf{M}_\kappa, \mathbf{C}, \mathbf{S}, \widetilde{\mathbf{C}}, \widetilde{\mathbf{S}}),$$

e.g. on gets $\mathbf{A} = \widetilde{\mathbf{S}}\mathbf{M}_\varepsilon\widetilde{\mathbf{S}}^T$ for electro-static or $\mathbf{A} = \widetilde{\mathbf{C}}\mathbf{M}_\nu\mathbf{C}$ for magneto-static problems, and thus can be projected onto a coarser grid by projecting the arguments of the expression. The incidence matrices on each grid level $(\mathbf{C}_h, \mathbf{S}_h, \widetilde{\mathbf{C}}_h, \widetilde{\mathbf{S}}_h)$ are directly available due to the grid incidence relations. The material matrices can either be constructed with the C-FIT modeler at each grid level or they can be obtained from merely algebraic projection operations from the C-FIT information on the finest grid with

$$\mathbf{M}_{h+i,\varepsilon} = \prod_{j=0}^{i-1} \mathbf{R}_{h+j,\widetilde{\mathbf{D}}_A}(\widetilde{\mathbf{D}}_{h,A}\mathbf{D}_{h,\varepsilon})\Big(\prod_{j=0}^{i-1} \mathbf{R}_{h+j,\mathbf{D}_L}\mathbf{D}_{h,L}\Big)^{-1} \tag{10}$$

$$\mathbf{M}_{h+i,\nu} = \prod_{j=0}^{i-1} \mathbf{R}_{h+j,\widetilde{\mathbf{D}}_L}(\widetilde{\mathbf{D}}_{h,L}\mathbf{D}_{h,\nu})\Big(\prod_{j=0}^{i-1} \mathbf{R}_{h+j,\mathbf{D}_A}\mathbf{D}_{h,A}\Big)^{-1}, \tag{11}$$

where

$$\mathbf{R}_{h,\mathbf{D}_L} := \mathbf{E}_h\mathbf{R}_{h,L}\mathbf{F}_h \;\;,\;\; \mathbf{R}_{h,\mathbf{D}_A} := \mathbf{E}_h\mathbf{R}_{h,A}\mathbf{F}_h \;\;,\;\; \widetilde{\mathbf{R}}_{h,\mathbf{D}_L} := \mathbf{E}_h\widetilde{\mathbf{R}}_{h,L}\mathbf{F}_h \;\;,\;\; \widetilde{\mathbf{R}}_{h,\mathbf{D}_A} := \mathbf{E}_h\widetilde{\mathbf{R}}_{h,A}\mathbf{F}_h, \tag{12}$$

using the linear maps $\mathbf{F}_h : \mathbb{R}^{3N_h \times 3N_h} \rightarrow \mathbb{R}^{3N_h}$ and $\mathbf{E}_h : \mathbb{R}^{3N_h} \rightarrow \mathbb{R}^{3N_h \times 3N_h}$, which are defined with $\mathbf{F}_h(\mathbf{A}) := \{\mathbf{A}_{i,i}\}$ and $\mathbf{E}_h(v) := \text{diag}\{v_i\}$ respectively. The projections method in (10) and (11) reflects the same geometrical considerations as described for the integral state variables. Eqn. (10) can also be used for the projection of $\mathbf{M}_\kappa$ by exchanging $\mathbf{D}_\varepsilon$ with $\mathbf{D}_\kappa$. The resulting projected material matrices are diagonal. Accordingly, the problem operators $\mathbf{A}_h$ can be constructed for each grid level from the problem discretized on the finest grid, with the transfer operators. This projection method is different to the Galerkin approach. In a first step it projects the problem geometry and discretization onto the coarse grid and consequently constructs the problem operators, i.e., only restriction operators are used in contrast to the Galerkin approach were also prolongation operators are involved. Although symmetric grid systems are used, the complete multigrid operation is non symmetric since $\mathbf{R}_h \neq \mathbf{P}_h$.

IV. Numerical Results

The MG scheme discussed above was implemented in MATLAB. In this paper we solve problems arising with discrete electro-static and magneto-static formulations using C-FIT. The geometry and material matrices for the finest grid and the grid information for all grid levels are created by a C-FIT 3D geometric modeler and imported into MATLAB. The coarse grid matrices are constructed according to (10) and (11). For the simulation a 1.8GHz Pentium III machine was used.

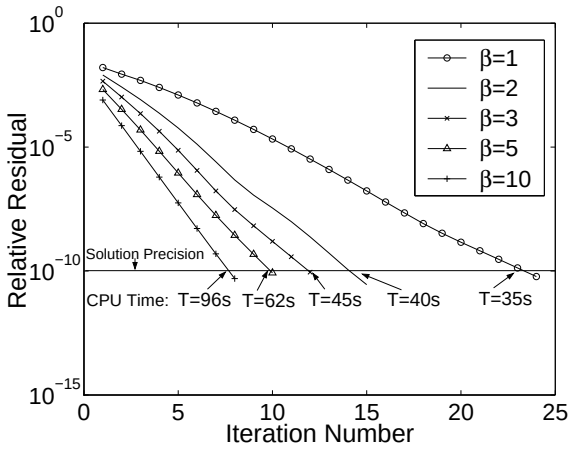

Fig. 7. Convergence history for different numbers of smoothing steps β.

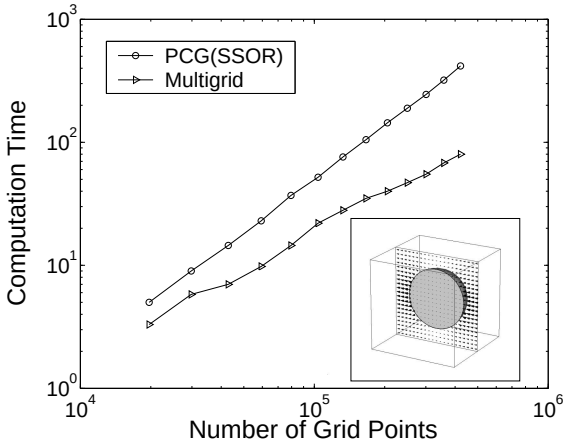

Fig. 8. Computation time in sec. versus number of grid points N_h for the solution of the test problem.

A. Electro-Statics

The formulation of discrete electro-static problems using C-FIT yields the linear algebraic Poisson system

$$-\nabla \cdot (\varepsilon \nabla \Phi) = Q \qquad \Longrightarrow \qquad \mathbf{A}\Phi = \widetilde{\mathbf{S}}\mathbf{M}_{\varepsilon}\widetilde{\mathbf{S}}^{T}\phi = \mathbf{q}. \tag{13}$$

The first test problem used for the numerical experiments is a plate capacitor containing a dielectric sphere ($\varepsilon_{\text{Sphere}} = 5\varepsilon_0$) embedded in vacuum ($\varepsilon_{\text{Vacuum}} = \varepsilon_0$). A mesh with $51 \times 51 \times 51$ grid points is used. Each coarser grid contains approximately half the number of grid points in each direction, which gives four grid levels, where the smallest grid consists of $7 \times 7 \times 7$ grid points. The geometry and the computed solution is contained in Fig. 8. The solution of this problem ($N_h = 132651$ grid points) could be computed down to machine precision (10^{-16}) solving the correction equation exactly on the smallest grid and using a Gauss-Seidel point-relaxation method with $\beta = 1$ at each grid level. The influence of β on the convergence characteristic is shown in Fig. 7. The total numbers of iterations decreases using more smoothing steps, but the total CPU time increases since more relaxation steps have to be computed in each iteration step. Hence for the following analysis $\beta = 1$ was chosen. To determine the asymptotic complexity of the solution method the test problem was solved for different grid sizes. The CPU time versus the number of mesh nodes

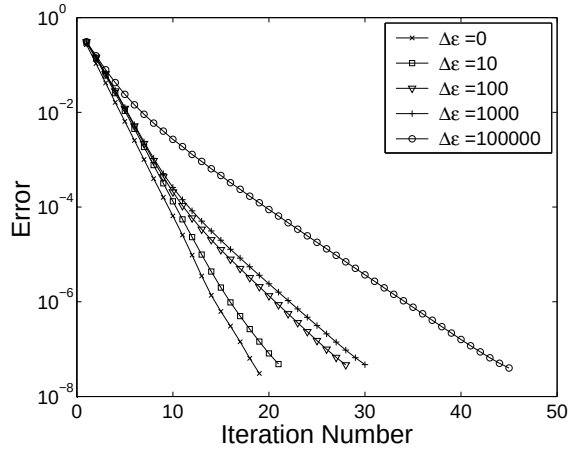

Fig. 9. Convergence history for different values of $\varepsilon_{\text{Sphere}}$ ($\Delta\varepsilon = \varepsilon_{\text{Sphere}} - \varepsilon_0$) .

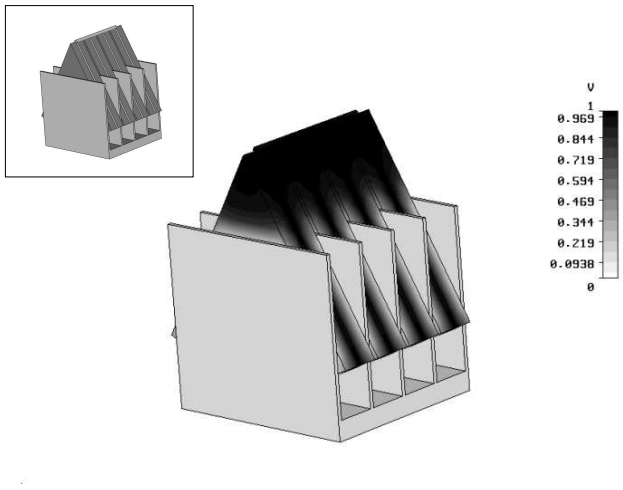

Fig. 10. Potential distribution of adjustable capacitor.

N_h is shown in Fig. 8. The slope in this log-log plot, i.e., the asymptotic complexity for $N_h \to \infty$, is determined to be 1.1 for the MG solver and 1.4 for the SSOR-preconditioned Conjugate Gradient (SSOR-CG) solver. Both values

do not entirely agree with the optimal theoretical expected values, which may be due to a non-optimal implementation within MATLAB. However the comparison to the SSOR-CG solver reveals an superior performance of the MG solution scheme for the discrete electrostatic problem.

The introduction of materials with large jumps in their coeffi cients leads to ill conditioned matrices $\mathbf{A}$ in (13). To study the influence of discontinuous material coeffi cients the test problem was solved using different values for $\varepsilon_{\text{Sphere}}$ (Fig. 9). To number of MG iterations needed to achieve convergence increases as expected. The asymptotic complexity of the MG solver, however, is not affected.

As a technical example, the MG solver is used to solve the 3D model of an adjustable multi-capacitor discretized with $55 \times 59 \times 50$ grid points (Fig. 10). The computation time of the MG solver is 80 s, whereas the computation time of the SSOR-CG solver is 140 s The solution was obtained with a relative residual norm of 10^{-8}.

B. Magneto-Static

More complicated problems arise with the magneto-static formulation of the C-FIT:

$$\nabla \times (\nu \nabla \times \vec{A}) = \vec{J} \qquad \Longrightarrow \qquad \mathbf{A}\widehat{\mathbf{a}} = \widetilde{\mathbf{C}}\mathbf{M}_\nu \mathbf{C}\widehat{\mathbf{a}} = \widehat{\widetilde{\mathbf{j}}}. \tag{14}$$

The formulation (14) represents a singular linear system of equations due to the non-trivial null space of the curl operators $\mathbf{C}, \widetilde{\mathbf{C}}$. The system is consistent thanks to the continuity equation $\nabla \cdot \vec{J} = 0$ which translates into the FIT as $\widetilde{\mathbf{S}}\widehat{\widetilde{\mathbf{j}}} = 0$. To maintain that the defect d_h lies in the range of $\mathbf{A_h}$, the restriction operator has to satisfy the relation

$$\widetilde{\mathbf{S}}_{h+1}\widetilde{\mathbf{R}}_{h,A} d_h = 0, \tag{15}$$

i.e., d_{h+1} is still free of divergence after the restriction. Using nested grids, relation (15) holds for the restriction operators introduced in section III. For general non-nested grids the restriction operators will not satisfy (15) and thus only an approximate correction can be obtained on the coarse grid. With a regularization of $\mathbf{A}_{h+1}$ to a matrix $\widehat{\mathbf{A}}_{h+1}$ in (14), it can be ensured that the right hand side vector $d_{h+1} = \mathbf{R}_h d_h$, where $d_h \in \text{Range}\{\mathbf{A}_h\}$ holds, lies in the range of $\widehat{\mathbf{A}}_{h+1}$. For this regularization, gauging methods such as graph theoretical tree-cotree techniques [9], a Grad-Div gauging [7] or an additional artifi cial mass term $\widehat{\mathbf{A}}_{h+1} = \mathbf{A}_{h+1} + \alpha\mathbf{M}$, ($\alpha > 0$), can be applied. Such a regularization is not applied in this paper. For the discrete system (14) a standard Gauss-Seidel smoother is applicable, since no additional (artifi cial) mass term $\mathbf{M}$ that extends (14) to $(\widetilde{\mathbf{C}}\mathbf{M}_\nu\mathbf{C} + \mathbf{M})\widehat{\mathbf{a}} = \widehat{\widetilde{\mathbf{j}}}$ requires that $\widetilde{\mathbf{S}}\mathbf{M}\widehat{\mathbf{a}} = 0$ has to be enforced by using either Hiptmair's divergence correction smoother [10] or the locally exact block patch smoother of Arnold, Falk and Winther [11]. Due to the discrete identity $\mathbf{C}\widetilde{\mathbf{S}}^T = 0$ any irrotational solution components of the solution $\widehat{\mathbf{a}}$ resulting from the non-trivial null space of $\mathbf{C}$ do not appear in the magnetic flux vector $\widehat{\widetilde{\mathbf{b}}} = \mathbf{C}\widehat{\mathbf{a}}$. For the

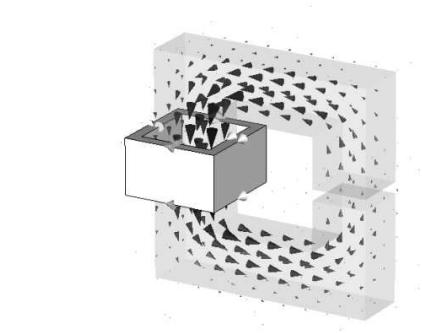

Fig. 11. Magnetic flux density in the C-magnet excited by a current coil obtained with the MG solver.

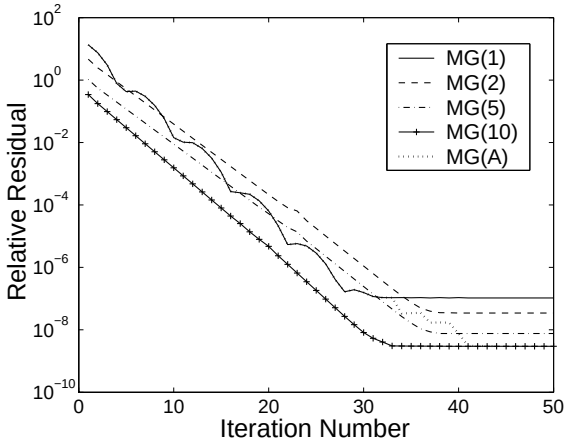

Fig. 12. Convergence history for different numbers of smoothing steps β labelled with MG(β) and for the adapted MG method MG(A).

following test problem also non-nested grids could be shown to be usable with suffi cient accuracy attainable. As a test problem the magnetic fi eld of a C-magnet excited by a current coil is simulated (see Fig. 11). The mesh size was

$N_h = 76900$ which leads to a matrix size of $3N_h = 230400$. The coarse grid dimensions were again chosen to be approximately half the number of grid points in each dimension, which leads to four grid level for this problem. Fig. 12 shows the convergence history of the MG solver for different numbers of smoothing steps. The solver stagnates at a relative residual of $3 \cdot 10^{-9}$. A SSOR-CG solver stagnates at approximately the same residual norm. For this magnetostatic test problem, the convergence characteristic shows an oscillatory behavior, which was also seen for an algebraic MG method for finite element discretizations [6]. However, when increasing the number of smoothing steps β, these oscillations disappear. Furthermore the obtained minimal residual norm also depends on β. Since the best convergence rate with respect to the consumed CPU time was achieved with $\beta = 1$, the number of smoothing steps is adaptively increased as soon as stagnation of the convergence occurs. In this way, the convergence of the MG scheme towards the maximal attainable accuracy can be maintained.

Using the same problem for varying values of the permeability $\mu_{\text{mag}} = \frac{1}{\nu_{\text{mag}}}$ of the iron core of the magnet, the oscillations in the convergence disappear with decreasing values for μ_{mag} (Fig. 13). Fig. 14 shows the CPU time for the test problem for different mesh sizes. In comparison to the SSOR-CG solver the MG solver shows an superior asymptotic complexity.

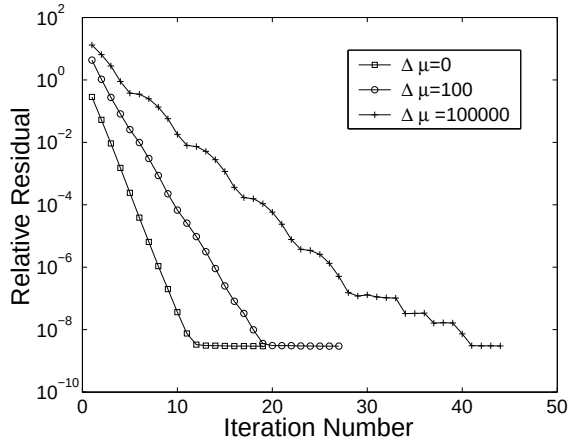

Fig. 13. Convergence history for different values of $\Delta\mu = \mu_{\text{mag}} - \mu_0$, representing a jump of material coefficients at an air-magnetic material interface.

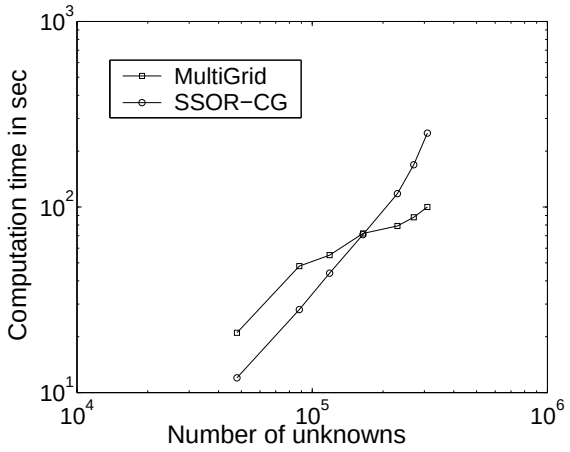

Fig. 14. Computation time for the C-magnet test problem versus number of unknowns.

V. Acknowledgements

The authors would like to thank Dr. Herbert De Gersem and Dr. Stefan Reitzinger for helpful comments.

References

[1] T. Weiland "A Discretization Method for the solution of Maxwell's Equations for Six-Components Fields", Electronics and Communications (AEÜ), Vol. 31, p. 116-120, 1977.

[2] B. Krietenstein, P. Thoma, R. Schuhmann and T. Weiland, "Facing the big challenge of high precision field computations", Proc. 19th LINAC conf., Chicago, August, 1998.

[3] W. Yu and R.Mittra, "A conformal finite difference Time domain technique for modeling curved dielectric surfaces", IEEE Microwave and Wireless Comp. Lett., Vol. 11, no. 1, pp. 25-27, 2001.

[4] A. Bossavit and L Kettunen, "Yee like schemes on staggered cellular grids: A synthesis between FIT and FEM approaches", IEEE Trans. Magn., Vol 36, no. 4, pp. 861-867, 2000.

[5] U. Trottenberg, C. Oosterlee, A. Schüller, "Multigrid", Academic Press, London, 2000.

[6] S. Reitzinger, J. Schöberl, "An algebraic multigrid method for finite element discretizations with edge elements", Numerical Linear Algebra with Applications, Volume 9, No 3, pages 223-238, 2002.

[7] M. Clemens and T. Weiland, "Regularization of eddy current formulations using discrete Grad-Div operators", IEEE Transactions on Magnetics, Vol. 38, No. 2, pp. 569-572, 2002.

[8] M. Clemens and T. Weiland, "Discrete electromagnetism with the Finite Integration Technique", Progress in Electromagnetic Research (PIER), no. 32, pp. 65-87, 2001.

[9] R. Rubinacci and G. Albanese, "Integral formulation for 3D eddy-current computation using edge elements", IEE Proceedings, Vol. 135, no. 7, p. 457, 1988.

[10] R. Hiptmair, "Multigrid method for in three dimensions", ETNA, 6 (1997), pp. 133-152.

[11] D. Arnold and R. Falk and R. Winther, "Multigrid in H(Div) and H(Curl)", Numerische Mathematik, Vol. 85, pp. 197–218, 2000.